Modeling of Formation of Helical Structures in Reversed-Field Pinch[*)]

Naoki MIZUGUCHI[1,2)], Akio SANPEI[3)], Shinichi FUJITA[3)], Kensuke OKI[3)], Haruhiko HIMURA[3)],
Sadao MASAMUNE[3)] and Katsuji ICHIGUCHI[1,2)]

[1)]*National Institute for Fusion Science, Toki 509-5292, Japan*
[2)]*The Graduate University for Advanced Studies (Sokendai), Toki 509-5292, Japan*
[3)]*Kyoto Institute of Technology, Kyoto, Kyoto 606-8585, Japan*

Nonlinear three-dimensional magnetohydrodynamic(MHD) simulations were applied to a reversed-field pinch(RFP) plasma to reveal the physical mechanism of the formation of helical structures such as the so-called quasi-single helicity and single helical axis states. The simulations were executed using the MHD Infrastructure for Plasma Simulation (MIPS) code in a realistic experimental geometry of the REversed field pinch of Low-Aspect ratio eXperiment (RELAX) device with reconstructed initial equilibria calculated by the RELAXFit code. Long-term evolutions showed remarkable formation of $n = 4$ structures as a result of the dominant growth of resistive modes. The resultant relaxed helical state consists of a bean-shaped, hollow pressure profile in the poloidal cross section for both the cases of resonant and non-resonant triggering instabilities.

1. Introduction

The reversed-field pinch (RFP) is an elaborate toroidal confinement concept, in which plasma is sustained by exploiting its constructive nature with a simple, compact magnetic system. The configurations can contain high-beta plasma with an intrinsically large toroidal current, which simultaneously provides effective Ohmic heating for a potential reactor. On the other hand, the system tends to be destabilized for the tearing mode instabilities in the core region because of the large current and the adjacent rational magnetic surfaces. The existence of multiple rational surfaces can cause interactions among the modes and chaotizing of the field lines. To avoid this degradation of the confinement, a passive control method is examined experimentally. By concentrating most of the mode activity into a single mode, a large magnetic island, in which the confinement property is improved, is formed in the core region. Several types of such states with a small number of helicity modes have been observed experimentally [1, 2], i.e., the quasi-single helicity (QSH), in which almost all the activities converge into a single mode, or the single-helical-axis (SHAx) state, in which the secondary arising O-point forms another three-dimensional magnetic axis. In the REversed field pinch of Low-Aspect ratio eXperiment (RELAX) [3], formation and rotation of helical structure have been observed [2].

In this study, we apply the nonlinear three-

dimensional magnetohydrodynamic (MHD) simulation approach which has been well established for modeling of the tokamak or helical plasmas [4, 5] to the RFP system. By reproducing the process of helical structure formation in the simulation, we aim to reveal the physical mechanism of the formation of helical structures in RFP. In this paper, the initial results of the simulation are reported.

In Sec. 2, the numerical model is explained. The simulation results are described by investigating the dynamical mechanisms in detail in Sec. 3. In particular, the formation of a unique three-dimensional structure and the effect of its trigger with the resonant and non-resonant instability modes are stated. The modeling is summarized in Sec. 4.

2. Simulation Model

To investigate the dynamical behavior of RFP plasma on the structural changes within the MHD time scale on the order of sub-millisecond, we solve a standard set of the nonlinear, resistive, and compressive MHD equations:

$$\frac{\partial \rho}{\partial t} = -\nabla \cdot (\rho \boldsymbol{v}), \tag{1}$$

$$\rho \frac{\partial \boldsymbol{v}}{\partial t} = -\rho \omega \times \boldsymbol{v} - \rho \nabla \left(\frac{v^2}{2}\right) - \nabla p + \boldsymbol{j} \times \boldsymbol{B}$$
$$+ \frac{4}{3}\nabla[\nu\rho(\nabla \cdot \boldsymbol{v})] - \nabla \times [\nu\rho\omega], \tag{2}$$

$$\frac{\partial \boldsymbol{B}}{\partial t} = -\nabla \times \boldsymbol{E}, \tag{3}$$

$$\frac{\partial p}{\partial t} = -\nabla \cdot (p\boldsymbol{v}) - (\gamma - 1)p\nabla \cdot \boldsymbol{v}$$

$$+ (\gamma - 1)[\nu\rho\omega^2 + \frac{4}{3}\nu\rho(\nabla \cdot \boldsymbol{v})^2 + \eta\boldsymbol{j}^2], \tag{4}$$

$$\boldsymbol{E} = -\boldsymbol{v} \times \boldsymbol{B} + \eta\boldsymbol{j}, \tag{5}$$

$$\boldsymbol{j} = \frac{1}{\mu_0}\nabla \times \boldsymbol{B}, \tag{6}$$

$$\boldsymbol{\omega} = \nabla \times \boldsymbol{v}. \tag{7}$$

The time development of the mass density ρ, velocity, $\boldsymbol{v}$, magnetic field $\boldsymbol{B}$, and pressure p are solved explicitly with the fourth-order finite difference and Runge-Kutta schemes using the MHD Infrastructure for Plasma Simulation (MIPS) code [6]. Viscosity ν and resistivity η are assumed to be uniform constants. In the original version of MIPS, the contribution of the net equilibrium current j_{eq} is subtracted to make the MHD equilibrium consistent with finite resistivity. However, here we evaluated the net current because in this simulation, the net plasma current changes substantially and plays a role in the MHD processes of interest.

The equations are solved in a cylindrical full-toroidal coordinate with a rectangular mesh in the poloidal plane. The grid size is (112, 112) for the poloidal plane and 128 for the toroidal direction, which was confirmed to be sufficient to converge numerically and resolve the physics described in this paper.

The initial conditions for the simulation are given by a numerical equilibrium that roughly follows the experimental conditions of RELAX. The equilibria are calculated by the Grad-Shafranov solver with a fitting reconstruction, the RELAXFit code [7]. The major and minor radii are 0.51 and 0.25 m, respectively. Several cases were examined for $1.5 < \Theta < 2.9$ and $-1.0 < F < 0.12$, where Θ and F represent the pinch and the field-reversal parameters, respectively. The results for two typical cases are stated in this paper. The first case, Case C, includes the $q = 1/4$ rational surface, where q is the safety factor, whereas the second case, Case D, does not, as shown in Fig. 1. The equilibrium parameters are $(\Theta, F) = (1.7, 0.0)$ for Case C, and $(1.9, -0.39)$ for Case D.

The boundary condition for the simulation differs slightly from that in the original version of MIPS. Essentially, the RFP is sustained with a stabilizing metal shell located near the plasma. Without the shell, the system becomes unstable to external modes both experimentally and numerically. To model this effect, all the quantities are fixed at a radius of 0.26 m from the geometrical center. The undesirable external modes were confirmed to be effectively suppressed by this treatment.

3. Results and Discussion

Small perturbations applied to the initial equilibria grow exponentially under finite resistivity. Here we use the parameters $\eta = 1 \times 10^{-5}$ and $\nu = 8 \times 10^{-4}$ to obtain an appropriate and numerically stable solution. For Case C, the
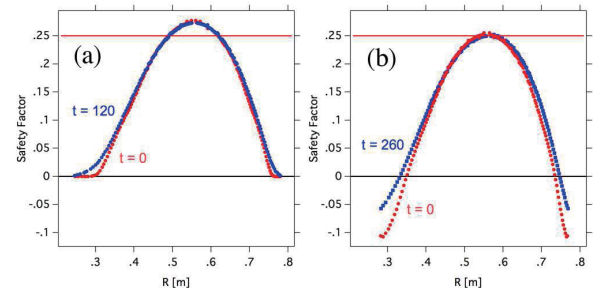
Fig. 1   Radial safety factor profile for (a) Case C and (b) Case D. Red lines indicate the safety factors for the initial state. Blue lines represent ones for the onset of the growth of linear instability modes.
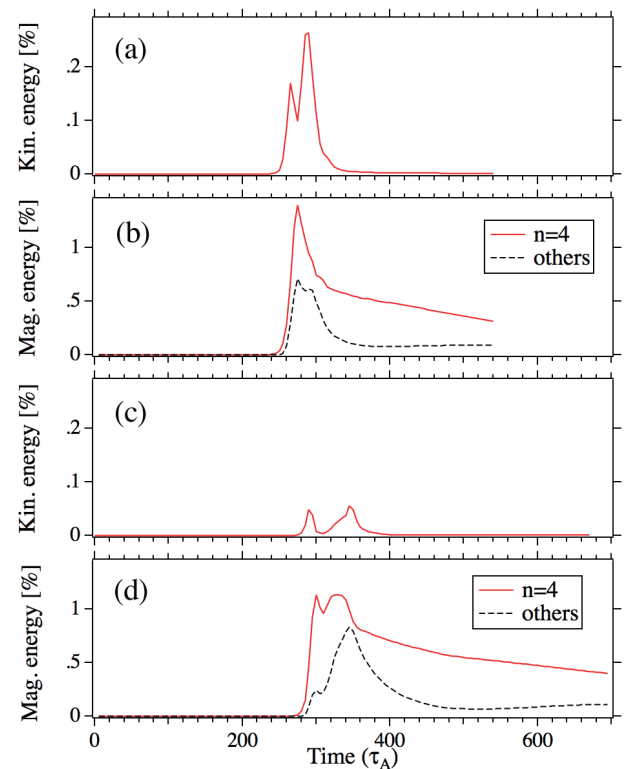
Fig. 2   Time development of total kinetic and magnetic energy of perturbations for Case C [(a)(b)], and Case D [(c)(d)]. Each energy is normalized by the initial total magnetic energy.

$n = 4$ component, where n is the toroidal mode number, dominates the linear growth compared to the other modes. The time development of the energy of the perturbations is plotted in Figs. 2 (a) and (b). The perturbation becomes visible scale at around $t = 240\,\tau_A$, where τ_A is the Alfven transit time which corresponds to 0.7 μsec for the operation parameter of RELAX. One can see from Fig. 2 (a) that the system undergoes relaxations with two peaks at $t = 260$ and $300\,\tau_A$ before the long-duration dissipative phase. The first is highly dominated by the $n = 4$ component, and the second includes considerable amount of other modes, as shown in Fig. 2 (b).
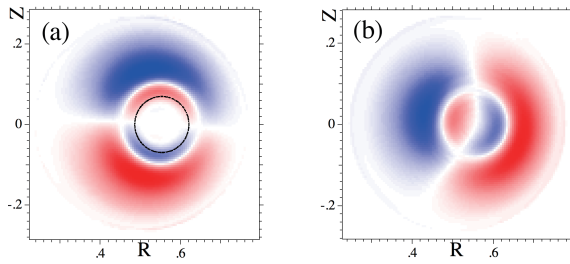
Fig. 3 Linear eigenmodes for the $n = 4$ mode for (a) Case C and (b) Case D. Perturbations in pressure are plotted with color contours. Position of $q = 1/4$ rational surface is indicated by the black line in (a).

The corresponding linear eigenmode structure of the $n = 4$ component is plotted in Fig. 3 (a). The $m = 1$ perturbation extends globally in the core region, where m is the poloidal mode number. The $q = 1/4$ rational surface is also plotted in Fig. 3 (a). The patterns appear to extend on and out of the $q = 1/4$ surface, i.e., to extend broadly over the $q < 1/4$ regions. Here the q profile is evaluated just before the onset of the linear modes, which are plotted with blue lines in Fig. 1. These modes have the nature of the resistive modes in that their growth rate increases at larger resistivity.

For Case D, on the other hand, the behaviors are unexpectedly similar to those in Case C, in which the $n = 4$ component is still most dominant in the linear stage, and two peaks appear for kinetic energy, as shown in Figs. 2 (c) and (d). The poloidal mode pattern plotted in Fig. 3 (b) is similar to that for Case C. In this case, the patterns extend over the entire poloidal cross section, because there is no $q = 1/4$ rational surface; i.e., $q < 1/4$ everywhere. Moreover, the behavior around the edge region does not qualitatively affect the overall process despite the difference in the edge q profile or the field-reversal parameter between the two cases.

This dominant growth of the $m = 1 / n = 4$ component for a wide range of parameters and profiles agrees qualitatively with experimental observations in RELAX, in which QSH states of the 1/4 mode appear periodically with suppression of the other modes [8].

One can expect from the mode patterns shown in Fig. 3 that a large $m = 1$ eddy flow can be induced in the poloidal cross section from the low-pressure (blue) toward the high-pressure (red) region. This flow may deform the core plasma into a bean-like shape as the amplitude of the perturbations increases.

This nonlinear time evolution is visualized in Fig. 4. The torus relaxes into a helically-twisted shape with four toroidal periods between the two energy peaks, as shown in Fig. 4 (a). The corresponding changes in the poloidal cross section are shown in Figs. 4 (b)-(g) and (h)-(j) for Cases D and C, respectively, with color contours of the pressure. In both cases, the poloidal contour deforms gradually into a bean-shaped structure, reflecting the linear eigenmode
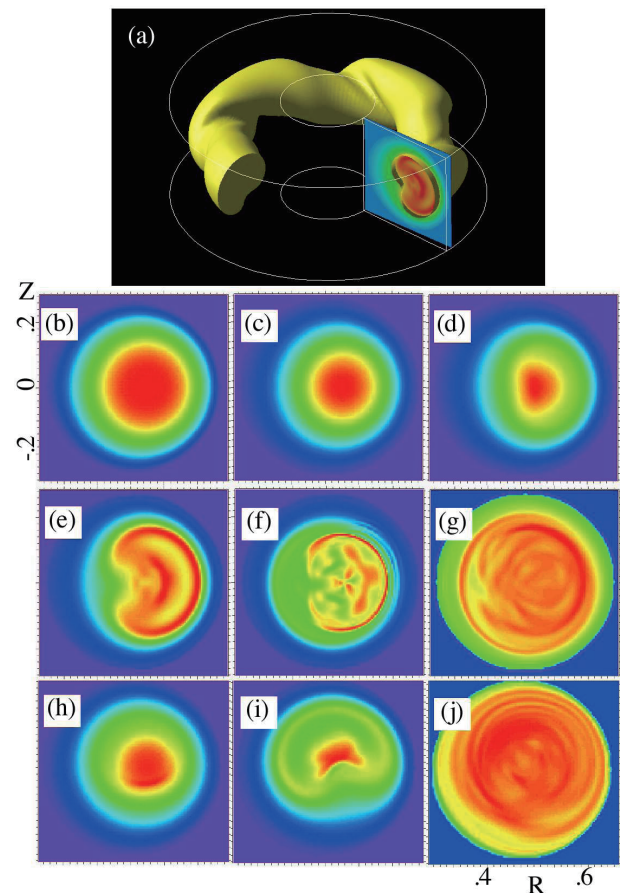
Fig. 4 Nonlinear time development of pressure profiles. (a)The bird's-eye view of an iso-pressure surface at $t = 305\,\tau_A$ for Case D. Poloidal contour map of the pressure at (b) $t = 0$, (c) 265, (d) 285, (e) 305, (f) 335, and (g) 695 τ_A for Case D, and (h) 255, (i) 265, and (j) 400 τ_A for Case C.

structure with the $m = 1$ component. In the relaxed states for both cases [Figs. 4 (e) and (i)], each of the poloidal pressure profiles becomes a highly hollow, deformed ring with a large crescent-shaped hole. Such a hollow bean-shaped helical structure was observed for a wide range of parameters and profiles in the simulation in addition to the two cases presented here, implying that such a structure stays under a type of minimal energy state.

After a brief pause at the helical structure, the system begins to develop again toward a more disordered profile with many small structures, as shown in Figs. 4 (f) and (j). Finally, the system reaches to a flatter profile during a lengthy dissipation phase.

The helical structures are thus created after the growth and saturation of the single $n = 4$ resistive instability for both cases into a unique structure with a bean-shaped ring on the poloidal cross section. Next, let us consider the temporal change in the magnetic configurations. For Case C, the linear instability grows resonant to the $q = 1/4$ rational surface, as shown in Fig. 5 (a). A large, single magnetic island is clearly formed on the $q = 1/4$ surface and grows
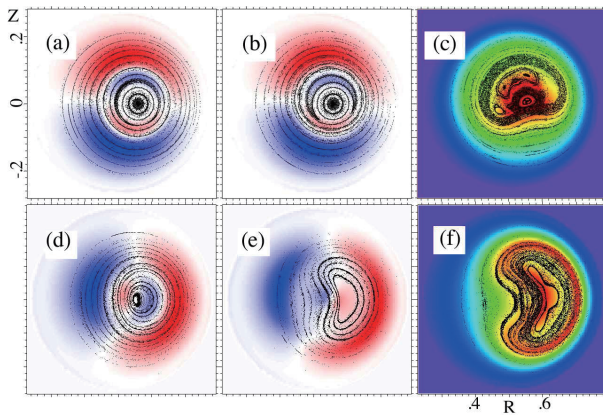
Fig. 5 Time development of the magnetic configuration. Puncture plots of the magnetic field at $t = 240$ (a), 250 (b), and $260\,\tau_A$ (c) for Case C and $t = 280$ (d), 290 (e), and $300\,\tau_A$ (f) for Case D are shown on the color contours of the $n = 4$-component [(a),(b),(d), and (e)] and the net [(c) and (f)] pressure.

in size [Fig. 5 (b)], demonstrating typical behavior of the tearing modes. On the other hand, the original magnetic axis shrinks gradually, whereas the created O-point of the island forms a new magnetic axis. Finally, the contour of the iso-pressure surface follows the magnetic surfaces of the created island, as shown in Fig. 5 (c). This mechanism of the structural change into a helical state has been recognized as the mechanism of QSH or SHAx states [9, 10].

However, in absence of the resonant $q = 1/4$ surface, i.e., Case D in this simulation, a similar helical structure is still formed in the relaxation process. Figures 5 (d)-(f) show the time evolution for Case D. The cross section deforms into a bean shape owing to the $m = 1$ flows of the kink-like resistive mode [Fig. 5 (d)]. The original nested surfaces are then largely deformed [Fig. 5 (e)] directly without any magnetic island formation. This mechanism based on the non-resonant instability provides us with a new model for understanding the formation of the helical RFP state without rational surfaces.

Finally, in both cases, the core pressure flows out along the deformed magnetic field lines, probably through a magnetic reconnection process between the core and the bean-shaped surface region. The resultant pressure profile forms a bean-shaped ring [Figs. 5 (c) and (f)].

4. Summary

Nonlinear three-dimensional MHD simulations were executed to reveal the physical mechanism of the formation of helical structures in an RFP plasma. The initial simulation results successfully reproduced the basic nature of the experimentally observed helical structures in RELAX

with the $n = 4$ component. Such helical structures can be formed both with and without a resonant rational surface. In addition, the simulation results imply that there can be a unique helical relaxed state in an RFP with a bean-shaped hollow pressure profile in the poloidal cross section.

To verify the simulation results by comparing them with the experimental observations in greater detail, and further analyze the properties of the relaxed three-dimensional state are our ongoing subject. Physically, the RFP can be a good application to explore the self-organized three-dimensional state in toroidal plasmas. By comparing the simulation with conventional relaxation theories, our understandings in this field would be advanced. Moreover, detailed linear analyses of non-resonant instabilities under the strong effect of the plasma current would improve the theory describing non-resonant resistive instabilities [11]. These topics remain as our future research.

[1] R. Lorenzini, E. Martines, P. Piovesan, D. Terranova, P. Zanca et al., Nature Phys. **5**, 570 (2009).
[2] K. Oki, R. Ikezoe, T. Onchi, A. Sanpei, H. Himura, S. Masamune and R. Paccagnella, J. Phys. Soc. Jpn. **77**, 075005 (2008).
[3] S. Masamune, A. Sanpei, R. Ikezoe, T. Onchi et al., J. Phys. Soc. Jpn. **76**, 123501 (2007).
[4] N. Mizuguchi, R. Khan, T. Hayashi and N. Nakajima, Nucl. Fusion **47**, 579 (2007).
[5] N. Mizuguchi, Y. Suzuki and N. Ohyabu, Nucl. Fusion **49**, 095023 (2009).
[6] Y. Todo, N. Nakajima, M. Sato and H. Miura, Plasma Fusion Res. **5**, S2062 (2010).
[7] A. Sanpei, K. Oki, R. Ikezoe, T. Onchi et al., J. Phys. Soc. Jpn. **78**, 013501 (2009).
[8] R. Ikezoe, T. Onchi, K. Oki, A. Sanpei, H. Himura and S. Masamune, Plasma Fusion Res. **3**, 029 (2008).
[9] R. Lorenzini, D. Terranova, A. Alfier, P. Innocente, E. Martines, R. Pasqualotto and P. Zanca, Phys. Rev. Lett. **101**, 025005 (2008).
[10] M. Onofri, F. Malara and P. Veltri, Nucl. Fusion **50**, 055003 (2010).
[11] K. Ichiguchi, Y. Nakamura and M. Wakatani, Nucl. Fusion **31**, 2073 (1991).